Mechanism of Lift Increase of Cavitating Clark Y-11.7% Hydrofoil

[1]Wakana Tsuru*; [1]Yushin Ehara; [1]Soichiro Kitamura; [2]Satoshi Watanabe; [2]Shin-ichi Tsuda;

[1]Graduated School of Kyushu University, Fukuoka, Japan; [2]Kyushu University, Fukuoka, Japan

Abstract

It is known that the lift force produced by hydrofoil slightly increases with some amount of cavitation. In the present study, cavitating flow around a Clark Y-11.7% hydrofoil in a water tunnel is experimentally studied in order to understand the detailed mechanism of lift increase. The experiments are carried out in three angles of attack conditions; 2.0, 8.0 and 20.0 degrees and in various gas content conditions. Although, at 2.0 degrees, the cavitation appearance and time-averaged lift and drag force differ due to differences of gas content, only the cavitation appearance differs at 8.0 degrees. In addition, at 20.0 degrees, the lift and drag force increase just after the inception of cavitation.

Keywords: cavitation; Clark Y hydrofoil; lift increase

Introduction

It is known that the lift force produced by a single hydrofoil slightly increases with some amount of cavitation before the sudden drop of lift (lift breakdown) at some angles of attack. This has been qualitatively explained by the additional camber effect, since the streamline of working liquid changes where the sheet cavity forms [1]. However, such sheet cavitation is often unsteady and in some cases the periodic large-scale vertical cloud cavities are generated. In such cases, it seems to be difficult to explain the mechanism of lift increase due to cavitation by stationary "camber effect". In addition, it is important to note that an increase of lift force is difficult to be predicted by even well-developed cavitation model in CFD [2]. Previous studies in the past have shown that the lift increase is related to the cavitation pattern. Various factors are involved in the cavitation pattern, and in experiments of single hydrofoil, cavitation shows different appearance at various angles of attack [3]. In addition, the gas content in water also affects cavitation, and it is shown that there are differences in the lift characteristics and the aspect of cavitation by amount of dissolved air [4]. Therefore, it is necessary that the mechanism of lift increase is understood by conducting more-detailed experimental investigation considering the flow features such as boundary layer types as well as water quality.

The measurement of lift and drag forces and the observation of cavitation appearance have been carried out in various angles of attack and dissolved air conditions in order to investigate the mechanism of lift increase. In the present study, the appearance and time-averaged lift and drag force of three angles of attack is investigated, and at the angle of attack of 20 degrees, the mechanism of lift increase is investigated.

Experimental apparatus and method

Experiments are carried out in a closed-loop cavitation tunnel consisting of upstream tanks, a rectangular test section with the width of 200mm and the span of 81.5mm and a circulating pump. The transparent acrylic windows are set at one-side, top and bottom walls for easy access for visual observations. In the present study, a two-dimensional Clark Y-11.7% hydrofoil with the chord length of C=100 mm and the span of S=81.0 mm as shown in Fig. 1 (a) is used.

The lift and drag forces (F_L, F_D) are measured by the strain gauges attached to the cantilever supporting the test hydrofoil under the assumption in which the flow is symmetrical with respect to the span center. The sampling frequency is 1,000 Hz and the sampling time is 40 s, whereas the resonance frequencies of cantilever system are 208 Hz and 74 Hz in bending modes normal and tangential to the hydrofoil chord respectively. The time-averaged surface pressure distribution is measured using the hydrofoil with pressure holes as shown in Fig. 1(b). In the high-speed observation of cavitation appearance, only one camera is used with mirrors to record two views from two directions, the top and the side, simultaneously. The frame rate is 8,000 fps and total time of recording is 1s. The measurements of lift and drag forces are synchronously carried out with high-speed recording.

Figure 2 shows the dependence of boundary layer developing along the suction surface of test hydrofoil on the angle of attack α in non-cavitating conditions, which has been specified from the measured surface pressures and the

*Corresponding Author, Wakana Tsuru: tsuru.w.123@kyudai.jp

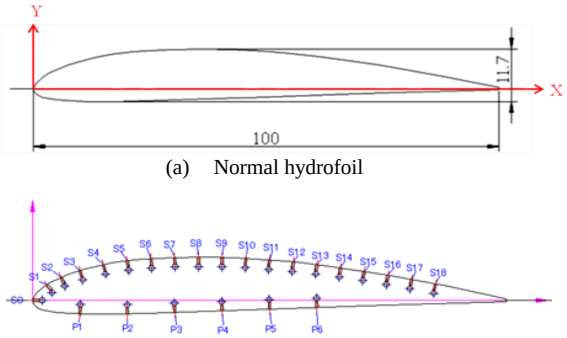

(a) Normal hydrofoil

(b) Hydrofoil with pressure taps

Figure 1 Clark Y-11.7% hydrofoil

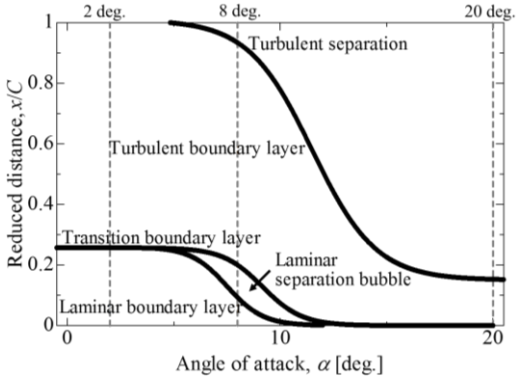

Figure 2 Boundary layer characteristics of suction side of Clark Y hydrofoil (Non-cavitation, R_e=4.5x10^5-1.0x10^6).

oil film visualizations. The surface limiting streamlines are observed from oil film composed of pigment, oleic acid, lubricant and grease after the operation with the main flow velocity of U=5.8m/s during 150s to 300s. From this chart, we have selected α=2.0, 8.0 and 20.0 degrees as the test conditions; at α =2.0 degrees, the laminar boundary layer smoothly transit to the turbulent one around the minimum pressure location. At α =8.0 degrees, the laminar separation bubble which promotes the turbulence transition forms near the leading edge of hydrofoil. At α =20.0, the turbulent flow separation occurs near the leading edge. The flow velocity is set to approximately U=8.1m/s at α =2.0 and 8.0 degrees, and U=5.8m/s at α=20.0 degrees. The gas content in water is evaluated by the amount of dissolved oxygen (DO) which is measured before and after every experiment. On the basis of measured DO value, we categorize the condition of gas content into three; high DO (70% or more of saturated value), medium DO (around 50%) and low DO (less than 30%) conditions.

The results are summarized in the non-dimensional forms using the cavitation number σ, the lift and drag coefficients C_L and C_D and blade surface pressure coefficient C_p, which are defined by $\sigma=(p_t-p_v)/0.5\rho U^2$, $C_L=F_L/0.5CS\rho U^2$, $C_D=F_D/0.5CS\rho U^2$ and $C_p=(p_x-p_t)/0.5\rho U^2$, respectively, where p_t is the test section pressure, p_v is the saturated vapor pressure, ρ is the water density, and F_L and F_D are lift and drag forces. Also, x is the distance in the chord length direction from the hydrofoil leading edge, and p_x is the blade surface pressure at x.

Results and discussion

Figure 3 shows the time-averaged lift and drag coefficients for α= 2.0, 8.0 and 20.0 degrees, respectively. The plots of red, green and blue show high DO condition, medium DO condition and low DO condition, respectively. In these figures, the inception cavitation number detected by naked eye observation is roughly indicated by the broken lines. The inception cavitation number is defined as the cavitation number when the cavitation occurs on the blade surface and cavitation growing begins.

At α=2.0 degrees, the drag force increases just after the inception of cavitation in the high and medium DO conditions, and at the same instance the lift force starts to decrease. On the other hand, in the low DO condition, the increase of the drag force is not seen and the lift force decrease is delayed to lower cavitation number. In addition, as shown in Fig. 4, in the high and medium DO conditions, many traveling bubble cavitations are observed, whereas in

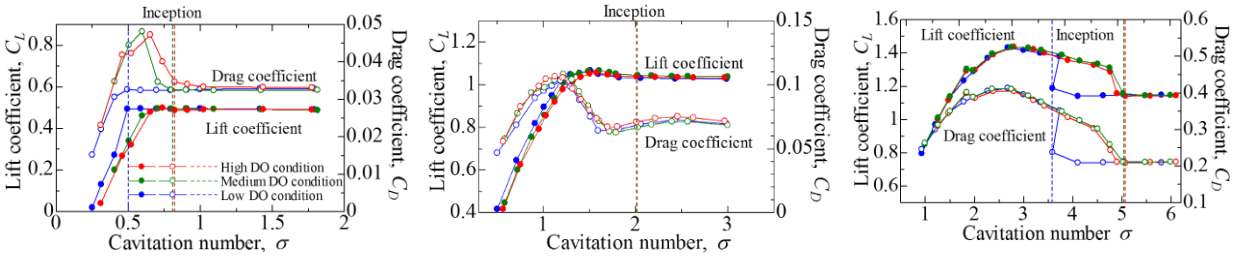

(a) α= 2.0 degrees. (b) α= 8.0 degrees. (c) α= 20.0 degrees.

Figure 3 Lift and drag coefficient curves for different gas content conditions.

*Corresponding Author, Wakana Tsuru: tsuru.w.123@kyudai.jp

the low DO condition sheet cavitation forms immediately after the inception. The increase of drag coefficient at high and medium DO conditions are supposed to be caused by the increase of momentum defect due to such bubble cavitations.

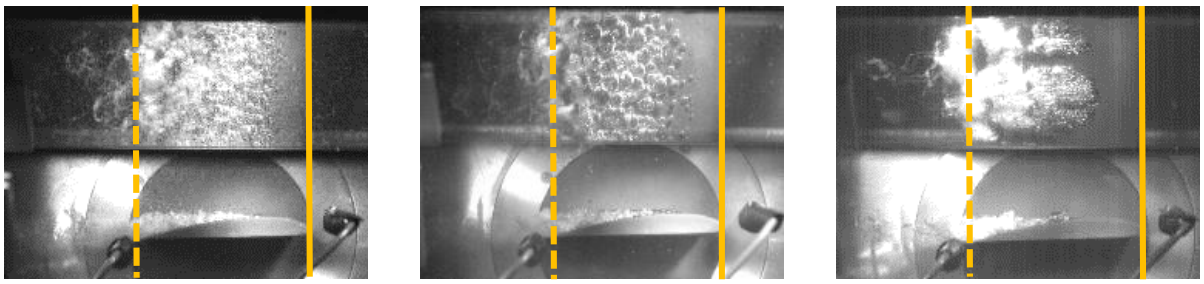

(a) High DO condition (σ=0.46) (b) Medium DO condition (σ=0.41) (c) Low DO condition (σ=0.40)

Figure 4 Cavity pattern in various DO conditions at α=2.0 degrees.

At α=8.0 degrees, in all DO conditions, the lift coefficient increases slightly after the inception of cavitation and decreases suddenly from around σ=1.3 at which the sheet cavity shows the strong unsteadiness due to the large-scale cloud cavity shedding. However, the appearance of cavitation is very different with the amount of gas content as shown in Fig. 5. Sheet cavitation consists of many travelling bubbles in the high and medium DO conditions, while the streak or film-like sheet cavitation is observed in the low DO condition. It is surprising that the influences of gas content on the time-averaged lift and drag coefficients as well as on the cavitation inception are small despite the different appearance of cavitation.

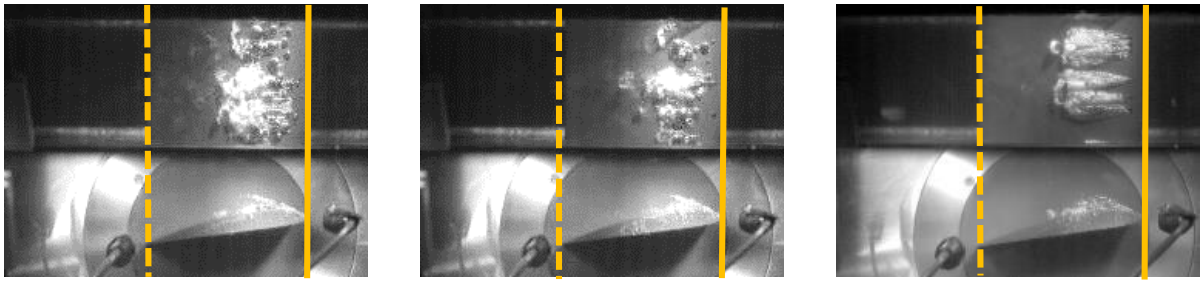

(a) High DO condition (σ=1.50) (b) Medium DO condition (σ=1.57) (c) Low DO condition (σ=1.51)

Figure 5 Cavity pattern in various DO conditions at α=8.0 degrees.

At α=20.0 degrees, as shown in Fig. 3(c), sudden increases of the lift and drag coefficients are observed immediately after the cavitation inception, and they reach the maximum value around σ=2.7. In addition, in the low DO condition, both the inception cavitation numbers and the cavitation number at the sudden decreases of lift and drag forces are small compared in the high and medium DO conditions. Figure 6 shows the blade surface pressure distributions in non-cavitating and cavitating conditions with large gas content. It can be seen that the pressure distribution changes all over the suction surface just after the inception of cavitation. In particular, in cavitation conditions, the minimum pressure is much larger than the vapor pressure as can be understood from $-C_{p,min}<\sigma$ ($C_{p,min}$ is the pressure coefficient at the suction peak). This indicates that the flow is highly unsteady, otherwise, we must not observe any cavitation bubbles in such a high pressure condition. Actually, Fig. 7 shows the cavity patterns and the time histories of lift and drag coefficients at σ=2.7 in the low DO condition, from which we can see the clear and significant periodic phenomenon; the cavity occurs from the leading edge of hydrofoil disappears after it has grown to a certain size. The lift and drag coefficients significantly fluctuate at the frequency corresponding to the cavity oscillations. In addition, as shown in Fig. 7, the lift and drag coefficients when there is no cavitation on the blade surface is approximately equal to those in non-cavitating condition. Although the results are not shown due to the limited space, it is confirmed that, as the cavitation number is decreased, the volume of cavity increases, and the fluctuation amplitudes and frequency of lift and drag coefficients also increase. The difference of cavity appearance and time histories of lift and drag coefficients due to the difference of DO are hardly observed once the cavitation starts to occur.

*Corresponding Author, Wakana Tsuru: tsuru.w.123@kyudai.jp

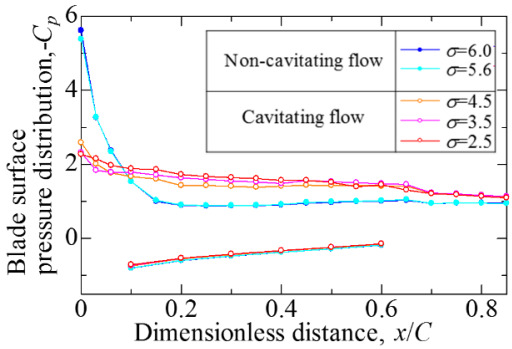

Figure 6 Surface pressure distributions at α=20.0 degrees.

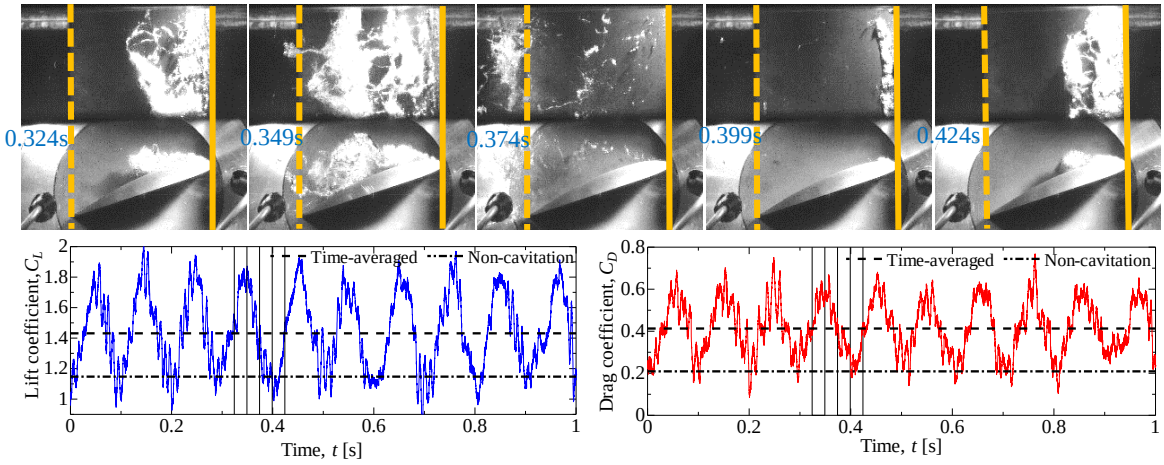

Figure 7 Cavity patterns and the corresponding lift and drag coefficients fluctuations at α=20.0 degrees (σ=2.7).

Conclusion

The mechanism of lift increase of a single hydrofoil with some occurrence of cavitation is investigated under the angles of attack of 2.0, 8.0 and 20.0 degrees where the boundary layer characteristics is different. The effect of gas content is also examined. Results are summarized as follows:

1. At the angle of attack of 2.0 degrees at which laminar to turbulent boundary layer transition occurs around the minimum pressure location, the influence of dissolved air is observed in both the appearance of cavitation and lift and drag characteristics.
2. At the angle of attack of 8.0 degrees at which the laminar separation bubble forms near the leading edge of hydrofoil, the difference due to the gas content is hardly observed in the time averaged lift coefficients although the cavitation appearance is so different.
3. At the angle of attack of 20.0 degrees at which the turbulent flow separation occurs near the leading edge, the blade surface pressure distribution and the time-averaged lift and drag forces significantly change once the cavitation occurs. This is seen regardless of the gas content, although the inception cavitation number is different. In addition, the lift and drag forces fluctuate greatly with the growth and extinction of the cavitation on the blade surface, resulting in the increases of time-averaged lift and drag coefficients.

References

[1] Knapp, R. T., Daily, J. W., Hammitt, F. G. (1970). *Cavitation*. McGraw-Hill.
[2] Kato, C., (2011). *Industry-university collaborative project on numerical predictions of cavitating flows in hydraulic machinery*. ASME-JSME-KSME Joint Fluids Engineering Conference 2011. AJK2011-06084. pp. 445-453
[3] Franc, J.-P., Michel J.-M. (2004). *Fundamentals of cavitation*. Kluwer Academic Publishers.
[4] Daido, H., Watanabe, S., Tsuda, S. (2015), *Effects of dissolved gas on unsteady cavitating flow around a Clark Y-11.7% hydrofoil*. ASME-JSME-KSME Joint Fluids Engineering Conference 2015. AJK2015-05488. V02AT05A006

*Corresponding Author, Wakana Tsuru: tsuru.w.123@kyudai.jp